ACS Combinatorial Science

Research Article

pubs.acs.org/acscombsci

Ag−ZnO Nanoreactor Grown on FTO Substrate Exhibiting High Heterogeneous Photocatalytic Efficiency

Sin Tee Tan,[†] Akrajas Ali Umar,*[,†] Aamna Balouch,[†] Suratun Nafisah,[†] Muhammad Yahaya,[†] Chi Chin Yap,[‡] Muhamad Mat Salleh,[†] I. V. Kityk,[§] and Munetaka Oyama[∥]

[†]Institute of Microengineering and Nanoelectronics, Universiti Kebangsaan Malaysia, 43600 Bangi, Selangor, Malaysia

[‡]School of Applied Physics, Faculty of Science and Technology, Universiti Kebangsaan Malaysia, 43600 Bangi, Selangor, Malaysia

[§]Electrical Engineering Department, Institute of Electronic System, Technical University of Czestochowa, 42-201 Czestochowa, Poland

[∥]Department of Materials Chemistry, Graduate School of Engineering, Kyoto University, Nishikyo-ku, Kyoto, 615-8520 Japan

ABSTRACT: This Research Article reports an unusually high efficiency heterogeneous photodegradation of methyl orange (MO) in the presence of Ag nanoparticle-loaded ZnO quasi-nanotube or nanoreactor (A-ZNRs) nanocatalyst grown on FTO substrate. In typical process, photodegradation efficiency of as high as 21.6% per μg per Watts of used catalyst and UV power can be normally obtained within only a 60-min reaction time from this system, which is 10^3 order higher than the reported results. This is equivalent to the turnover frequency of 360 mol mol^{-1} h^{-1}. High-density hexagonal A-ZNRs catalysts were grown directly on FTO substrate via a seed-mediated *microwave*-assisted hydrolysis growth process utilizing Ag nanoparticle of approximately 3 nm in size as nanoseed and mixture aqueous solution of $Zn(NO_3)\cdot 6H_2O$, hexamethylenetetramine (HMT), and $AgNO_3$ as the growth solution. A-ZNRs adopts hexagonal cross-section morphology with the inner surface of the reactor characterized by a rough and rugged structure. Transmission electron microscopy imaging shows the Ag nanoparticle grows interstitially in the ZnO nanoreactor structure. The high photocatalytic property of the A-ZNRs is associated with the highly active of inner side's surface of A-ZNRs and the oxidizing effect of Ag nanoparticle. The growth mechanism as well as the mechanism of the enhanced-photocatalytic performance of the A-ZNRs will be discussed.

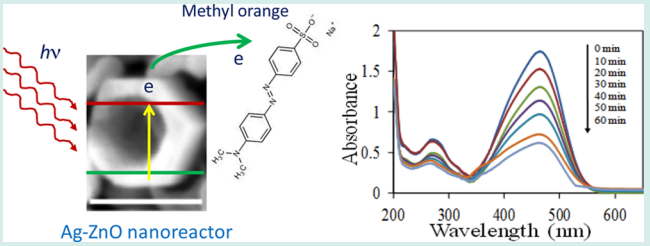

KEYWORDS: *Ag−ZnO nanoreactor, photocatalyst, heterogeneous, high-efficiency*

1. INTRODUCTION

Surface structure of nanocatalyst, such as crystal facet, defect, or kink site, etc., plays a key role in promoting surface reaction.[1] Synthesis of nanocatalyst with surface morphology containing a highly defective structure is believed to facilitate a facile and rapid catalysis process or surface reaction because of the high-density localized-electron on the surface.[1−6]

ZnO nanostructures are a widely used catalysts in many catalysis applications,[7,8] including water-splitting,[9] and degradation of organic pollutants,[10] such as methyl orange (MO),[11] methylene blue (MB),[12] and bisphenol A.[13] Despite the excellent catalytic performance obtained so far, however, their overall peformance, determined from the relative efficiency over mass of catalyst and UV light power used, is rather low. In a typical case, efficiency as high 0.28% per microgram catalyst per watt of UV light used is the highest performance reported so far in a homogeneous catalytic reaction using ZnO nanostructure with nanorod morphology.[14] Although a great deal of effort has been dedicated to improving the catalytic efficiency of ZnO nanostructure, mainly via synthesizing nanostructure with high surface area or controlled-morphology,[15] such as nanotubes, it has resulted in limited sucess.[16] Nanotubes, for example, have been well-known as the structures that offer a wide surface area for reaction because they have inside and outside surfaces. Nevertheless, the inside surface is has limited accessibilty for the reactant because of high-surface potential at the nanotube end, which increases with increasing nanotube aspect ratio, that hinders the reactant transport. Thus, the catalytic performance is kept limited.

Here, we present a simple method to produce ZnO nanostructure with novel morphology directly on the substrate surface, namely, quasi-nanotube or nanoreactor with a large number of defects in the inside surface and loaded with Ag nanoparticles using a microwave-assisted hydrolysis process. The Ag nanoparticle-loaded ZnO nanoreactor (A-ZNRs) has a length and outer and inner diameters of approximately 120, 100, and 90 nm, respectively. With relatively wide diameter and low-aspect ratio, the structure grants excellent reactant accessibility, allowing the reactant to enter the nanoreactor and come in contact with the inside surface. Thus, excellent

Received: December 9, 2013
Revised: March 30, 2014
Published: June 11, 2014

photocatalytic properties are predicted to be obtained from this nanostructure. Ag nanoparticle loading may further expand the catalytic performance of the ZNR system because it may lead to the increase of the oxidation state of the ZnO nanostructure as a result of the increase of the electron valence, which may induce active redox reaction. This process could also enlongate the lifetime of the excited electrons at the conduction band and improve the charge transfer characteristic of the ZnO nanostructure. Thus, enhanced photocatalytic performance is expected to be obtained. The hetereogeneous catalytic property of the A-ZNRs has been evaluated in the photodegradation of methyl orange (MO). Photocatalytic efficiency as high as 25% μg^{-1} W^{-1} has been successfully obtained so far. This result is 10^3 order higher than recently reported result.[17−19] The A-ZNRs should find potential use in photolysis or photoelectrochemical reaction.

2. METHODOLOGY

2.1. Preparation of Ag Nanoparticle-Loaded ZnO Nanoreactor (A-ZNRs). A-ZNRs were synthesized via a seed-mediated microwave-assisted hydrolysis growth process, our previously reported method.[20,21] In the present approach, which is crucial for the formation of A-ZNRs, Ag nanoparticle of ∼3 nm in size instead of ZnO nanoseed was used. A previously reported metal seeding method[22−24] was applied in this experiment to prepare Ag nanoseed on the FTO substrate. Briefly, Ag nanoseeds were prepared on the FTO surface by first immersing the FTO substrate into a 20 mL solution that contains equimolar concentrations (0.25 mM) of silver nitrate (Sigma Aldrich, reagent grade) and trisodium citrate (Wako Pure Chemicals Ltd.) for 30 min. After that, 0.5 mL of 0.1 M ice-cooled $NaBH_4$ (Wako Pure Chemicals Ltd.) was added into the solution. The solution and the FTO substrate in it were then kept undisturbed for an hour at room temperature (∼25 °C). The substrate was then taken out, rinsed with a copious amount of pure water and finally dried with a flow of nitrogen gas. From this approach, high-density Ag nanoseed of size approximately 3 nm can be grown on the FTO substrate. The substrate was then annealed in air at 200 °C for 1 h to remove any organic compound on the surface.

The Ag nanoseed attached FTO substrate was then immersed into a Teflon shielded-glass vial containing equimolar (0.04 M) of zinc nitrate hexahydrate and hexamethylenetetramine (HMT) (Sigma aldrich, reagent grade) in the presence of variable concentration (2.5−15 mM) of silver nitrate (Sigma Aldrich, Reagent greade, 99%) solution for A-ZNRs growth process. The growth process was carried out under the influence of double-step microwave irradiance power, namely, 171 and 858 W in a Panasonic inverted home application microwave system (NN-GD577M, 1100 W, 2.45 GHz). The growth time was set for 10 and 20 s for first and second step microwave irradiation, respectively. The growth solution temperature during the growth process was monitored using a thermocouple. The sample was then taken out, cleaned with a copious amount of deionized water and dried with a flow of nitrogen gas. In this paper, the effect of microwave power as well as the effect of the double-step process on nanostructure growth will not be discussed. The optimum condition reported in our previous paper was adopted. Pure water with 18.2 MΩ resistance was used throughout the experiment and all the materials were used without any further purification.

2.2. Characterizations. The morphology of A-ZNRs was characterized by a field emission scanning electron mocroscope (FESEM) ZEISS Supra 55 VP that operated at the acceleration voltage of 3kV. The high resolution trasmission electron microscopy characterization was obtained from a ZEISS Libra 200 FE apparatus. The nanostructure phase was evaluated using X-ray Diffractometer (XRD) Bruker D8 with CuKα irradiation and scanning rate of 0.002 deg/s.

2.3. Photocatalytic Degradation of Methyl Orange (MO). The heterogeneous photocatalytic property of A-ZNRs was evaluated in the degradation of methyl orange (MO) under UV light irradiation. In a typical procedure, the A-ZNRs attached substrate was immersed into 20 ppm of MO aqueous solution and exposed on a continuous UV light irradiation of wavelength and power of 365 nm and 4 W, respectively. It needs to be noted here that the UV power used is much lower than that recently reported result and is meant to minimize the effect of UV radiation on the MO degradation and thus obtain the effectiveness of the catalytic property of ZnO nanostructure. During the experiment, the solution was continuously stirred at 100 rpm. The MO photodegradation dynamic was monitered by UV−vis Spectrometer Perkin-Elmer Lamda 900.

3. RESULT AND DISCUSSION

3.1. Ag Nanoparticle-Loaded ZnO Nanoreactor (A-ZNR) Synthesis and Characterization. Using the microwave hydrolysis approach, A-ZNRs were successfully grown directly on the FTO substrate. The result is shown in Figure 1. As seen

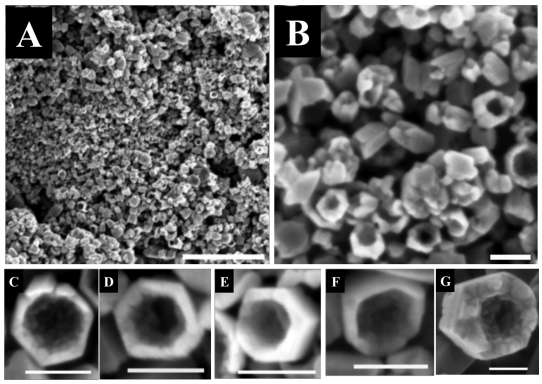

Figure 1. (A, B) Typical FESEM images of Ag nanoparticle-loaded ZnO nanoreactor (A-ZNRs) prepared using the growth solution that contains equimolar (0.04 M) of $Zn(NO_3)\cdot 6H_2O$ and HMT in the presence of 10.0 mM of $AgNO_3$. Total growth time was 30 s. (C−G) Typical morphology of A-ZNRs. Scale bars are 1 μm in A and 100 nm in B to G.

from Figure 1A and B, high density A-ZNRs have been successfully grown on the FTO surface, and using the image analysis (ImageJ) software, we calculated the surface coverage of the nanotube growth to be as high as 90.3%. From the image, it was also found that the A-ZNRs adopted hexagonal morphology (see Figure 1B), which is similar to the structure normally obtained using the hydrothermal method. The length of the nanotube was around 95 nm with shell thickness and a hexagonal edge length of approximately 15 and 40 nm, respectively. Interestingly, it is revealed from the high-resolution images in Figure 1C−G that the A-ZNRs is apparently highly rough or contains defects on the inner surface and on the end of the nanotubes, promising peculiar performance in applications because of the high density of high-energy atom sites. With an incomplete hollow structure of

dx.doi.org/10.1021/co400157m | ACS Comb. Sci. 2014, 16, 314−320

different depth, the A-ZNRs may behave as a nanoreactor for catalytic reactions.

As the surface structure of the A-ZNRs was characterized by a FESEM analysis, the bulk structure was examined using HRTEM. The result is shown in Figure 2. As shown in Figure

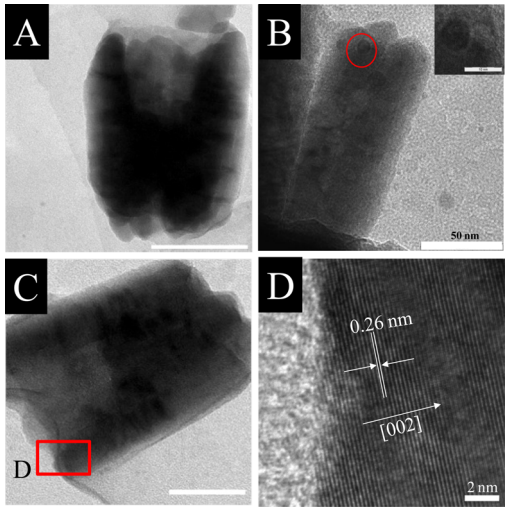

Figure 2. (A–C) Low-resolution TEM image of A-ZNRs. The red circle in B highlights the formation of the Ag nanoparticle interstitially grown in the A-ZNRs structure. (D) High-resolution TEM of ZNRs. Scale bars in A and C are 100 nm.

2A–C, the A-ZNRs exhibit a high-defect structure throughout the body of the A-ZNRs, particularly at the structure's end. This result agrees with the FESEM image as shown in Figure 1. Interestingly, dark spot structures are apparent in the A-ZNRs (see red circle and inset in Figure 2B). This is probably the Ag nanoparticles that are interstitially incorporated into the ZnO nanoreactor (ZNRs) structure that grows via a heterogeneous nucleation process. The presence of Ag nanostructure in the ZNRs is confirmed in the XRD analysis, which will be presented later. These defect's formations as well as the substitution of Ag nanoparticles into the structure promises distinguish photocatalytic activity. We further evaluated the nanocrystal growth property by taking a HRTEM image of the structure. However, despite the ZNRs being characterized by a high-defect structure on their surface as confirmed in the FESEM image and the low-resolution TEM analysis, surprisingly the ZNRs are single crystal in nature. This is confirmed by the presence of ordered-lattice fringe without the presence of twinning or dislocation. On the basis of the lattice fringe analysis, it is found that the crystal growth direction is toward the *c*-axis of ZnO crystal, namely [002], inferring that the ZNRs growth preparation using the presence condition adopts the normal stable wurtzite ZnO crystal phase (Figure 2D).

Figure 3 shows the X-ray diffraction data for the A-ZNRs. As can be seen from the figure, eight sharp peaks appear in the spectrum. By considering the presence of Ag in the nanostructure, as shown in the TEM image, we assumed that these peaks must belong to Ag and ZnO crystals. XRD diffraction data JCPDS file no. 04-0783 confirmed that the peaks at 2θ = 38°, 44°, and 52° belong to *fcc* Ag nanocrystal. And also, judging from the intensity of the peaks, we believed that the Ag nanoparticles should be grown in high-density on the surface, either interstitially inside the ZNRs structure or

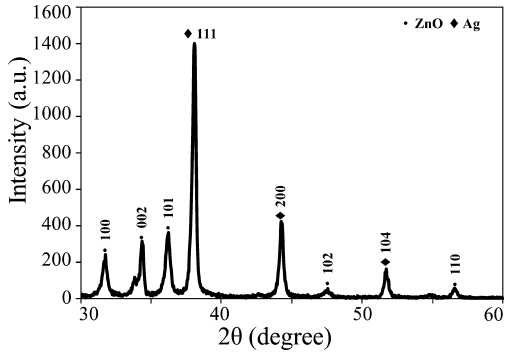

Figure 3. Typical X-ray diffraction spectra of Ag nanoparticle-loaded ZnO quasi-nanotube (A-ZNRs) showing the presence of Ag nanoparticles.

freestanding on the FTO substrate. This condition might then produce a peculiar catalytic property. Meanwhile, the other peaks, that is, at 2θ = 36.2°, 34.4°, 31.8°, 47.6°, and 56.6°, agreed with the XRD data JCPDS file no. 36-1451, namely, hexagonal wurtzite structure of ZnO, which correspond to (002), (100), (102) and (110) Bragg planes, respectively.

While the hexagonal shape of the nanotube can be related to common crystal growth morphology for ZnO grown from solution, the mechanism of tubular formation is not yet understood. However, this mechanism might be more or less similar to that of ref 25, namely, the effect of selective etching of an Ag^+ ion onto the (002) plane of ZnO under the influence of the microwave field. The following facts can be taken as clear evidence for such growth mechanism. First, the ZNRs may only form when Ag^+ ions are present in the growth solution and their concentration should be in the range of 8.0 and 15.0 mM. Lower or higher concentration leads to the formation of flower shape nanorods and deteriorated-nanoring, respectively (see Figure 4). No ZNRs was formed if the Ag^+ ions were absent. Instead, solid hexagonal nanorods were formed. Second, the depth and the diameter of the tubular structure increased with the greater level of Ag^+ concentration (see Figure 4C and 4D). Third, Ag nanoseed is critical in this process, where no

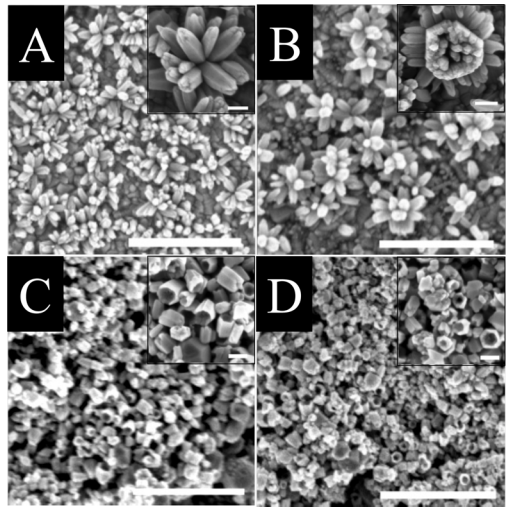

Figure 4. FESEM images of A-ZNRs grow in various $AgNO_3$ concentrations, namely, (A) 2.5, (B) 5.0, (C) 10.0, and (D) 15.0 mM. Other chemicals in the growth solution and the microwave irradiation parameter are kept unchanged. The growth time is 30 s.

dx.doi.org/10.1021/co400157m | *ACS Comb. Sci.* 2014, 16, 314–320

nanostructures were formed on the surface during such short growth process if Ag nanoseed was absence. The used of ZnO nanoseed instead of Ag only projects the formation of ZnO nanorods.

The A-ZNRs formation is very quick, apparently starting as early as 15 s, as judged from the FESEM image for ZnO nanostructure growth taken during the early growth process, as shown in Figure 5. For the structure to be formed, we predict

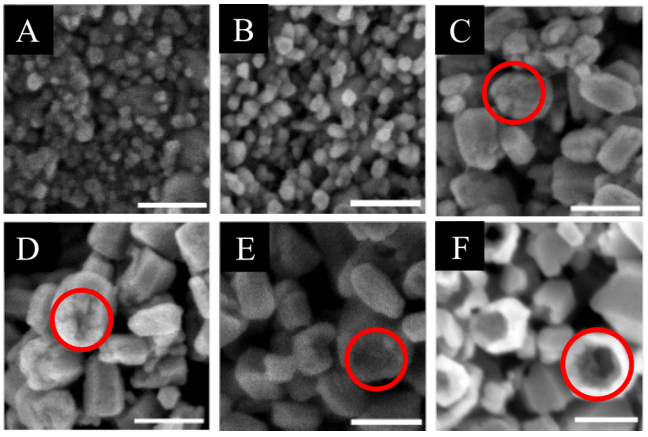

Figure 5. FESEM image of ZnO nanostructures prepared at different growth times: (A) 3, (B) 5, (C) 10, (D) 15, (E) 18, and (F) 20 s utilizing the optimum growth condition. Red circles show the etching process on the A-ZNRs. Scale bars are 100 nm.

that the hexagonal nanorods of ZnO must be formed on the FTO substrate immediately after the application of the microwave field on the reaction, probably in the period of less than 5 s (see Figure 5B). Such crystal growth is extremely fast. It is probably enabled by the presence of *fcc* crystal Ag nanoseed on the surface, which facilitates rapid nucleation of ZnO via a lattice mismatch process. It should be also considered that the etching process might also immediately take place when the crystal plane of ZnO is completely formed. We found that, within 10 s of reaction, deterioration on the hexagonal plane of the nanorod's end was observed (see the red circle in Figure 5C). However, we thought that the crystal plane's growth must be faster than the etching process in order to form a A-ZNRs structure. Judging from the microscopic analysis result, the oxidation of ZnO from the crystal plane should be initiated from the center of the (002) plane, which is the most unstable site in the hexagonal morphology.[26,27] The oxidation will produce Zn^{2+} and O^{2-} in the solution, which renucleates to promote the growth of the growing plane. The Ag^{+} itself will reduce to Ag^{0} and form Ag nanoparticles either in the solution or on the FTO substrate. The oxidation rate toward the short and long axis is considered to be comparable and the process will stop when the Ag^{+} has been consumed.

Nonetheless, the microwave power use, as well as the nature of its application during the growth process, such as continuous or double stepped-power, should also play a unique role in the growth process. However, in this study, the effect of microwave power on the formation of A-ZNRs, as well as its interplay with the Ag^{+} ion, was not studied. Since the formation of A-ZNRs is found to be merely due to the effect of Ag^{+} (see Figure 4), we thought that the microwave power presumably only influenced the rate of nanocrystals growth. However, the effect of microwave power use, as well as its interplay with Ag^{+} ion on the ZnO nanostructure's growth, is being studied and will be reported on in a different paper.

3.2. Photocatalytic Degradation of MO. The photocatalytic properties of A-ZNRs were examined in the photo reduction of methyl orange (MO). By immersion of the A-ZNRs sample into 20 mg/L of MO, the photocatalytic degradation of MO was recorded. Figure 6A shows the

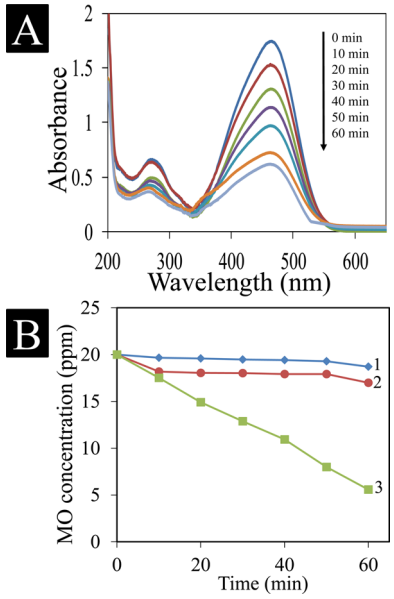

Figure 6. (A) Optical absorbance spectra of MO during the photodegradation process in the presence of two slides of A-ZNRs. (B) Photodegradation kinetic of MO in the absence of photocatalyst (1) and in the presence of ZnO nanorods (2) and two slides of Ag/ZnO quasi-nanotube (3) photocatalyst samples.

photodegradation kinetic of MO in the presence of two slides of A-ZNRs catalysts under a 4 W UV light exposure. As can be seen from Figure 6A, the optical density of MO at a wavelength of 463 nm decreased significantly with the elongation of the reaction time. As Figure 6A shows, the initial absorbance of MO is around 1.74. Surprisingly, it reduces to 0.52 within only 60 min. This is equivalent to degradation as high as 70%. This value is surprisingly high from the viewpoint of the heterogeneous catalytic process, reflecting the high-catalytic property of A-ZNRs. To further confirm the high catalytic performance of the A-ZNRs, the photodegradation kinetic of MO in the presence of undoped-ZnO nanorods (undoped-ZnO nanostructure has nanorods morphology) and in the absence of nanocatalyst sample were evaluated. The results are shown in Figure 6B. For the case of in the presence of undoped-ZnO nanorods, as can be seen from the curves (see curve 2), the degradation of MO is much lower compared to its degradation in the presence of A-ZNRs (curve 3), which only decrease as high as 15.1% for the designation reaction time of 60 min. Considering the mass of undoped-ZnO nanorods on the slide is much higher (even though only using one slide) compared to the two-slides of A-ZNRs, that is, 168 μg (0.812 μg for two slides of A-ZNRs for comparison) and the MO degradation value, it can be worth mentioned that the photocatalytic efficiency of A-ZNRs is approximately 1000 times higher than the undoped-ZnO nanorods. We then evaluated the extent of UV irradiation effect on the MO degradation. However, the result is quite low, namely 6.2% only

dx.doi.org/10.1021/co400157m | ACS Comb. Sci. 2014, 16, 314−320

(see curve 1) for the designated reaction time. Thus, these results further prove the excellent photocatalytic property of A-ZNRs system.

To compare the performance of the present system with the reported result, we have calculated the photocatalytic degradation efficiency of the A-ZNRs by using the relation[3,4] η = (% degradation)/(μg of catalyst)·$W_{UVpower}$, where % degradation, μg of catalyst, and $W_{UVpower}$ is the percent degradation at the final reaction time, mass of the A-ZNRs on the substrate surface in micrograms, and the power of UV light used in watts, correspondingly. The mass of ZnO on the surface involved in the oxidation reaction was calculated by considering the mass density, dimension of nanotube, density of the A-ZNRs on the surface and the total surface area. The mass of A-ZNRs on 1 slide is approximately 0.406 μg or 0.812 μg if two slides are used. Since the UV light power used in this study was 4 W, the photodegradation efficiency in our system is as high as 21.6% μg^{-1} W^{-1}, which is 10^3 times higher than the reported results[14,17,18] (see Table 1). We have analyzed the

Table 1. Efficiency of Photodegradation MO of A-ZNRs and Other System

	mass of ZnO particles (μg)	efficiency ((% degradation)/(μg of ZnO × $W_{UVpower}$)) at reaction time	UV power (W)	time of reaction (min)	ref
1	0.812	21.60	4	60	our data
2	325	0.28	14.3	100	14
3	5000	0.001	20	80	18
4	200000	0.0000022	125	120	17

turnover frequency (ToF) of the system. The ToF as high as 90 mol mol^{-1} h^{-1} was obtained. However, because only small part of A-ZNRs on the surface involved in the reaction, the ToF should be much higher from this value. By considering around 25% only of the A-ZNRs takes place in the catalytic reaction, the ToF become 360 mol mol^{-1} h^{-1}. In good agreement with the catalytic efficiency described above, the ToF value obtained here is also quite high in the viewpoint of heterogeneous catalysis process, confirming active catalytic property of A-ZNRs.

High photocatalytic efficiency in the present A-ZNRs could be related to the following facts: First, the presence of large-defect density both on the inner and the outer surfaces of the A-ZNRs that enable facile and active reaction on the surface with MO molecules. It is well-known that the catalytic and surface reactions actively occurred at the defect site or kinks structure. Second, it could also be related to high-surface area[28] of the A-ZNRs resulting from tubular morphology, thus providing a large site for adsorption of MO molecules. The nature of A-ZNRs with large inner diameter and low aspect ratio grant excellent surface accessibility by the MO onto both inner and outer surfaces of the A-ZNRs, thus enhancing effective surface reaction with the catalyst. Third, the presence of Ag nanocatalyst on the A-ZNRs structure as confirmed by the TEM image in Figure 2 could also be considered as the reason for the high-photocatalytic property because Ag nanocrystal may improve the light absorption as well as the oxidation energy of the A-ZNRs system, thus enhancing the charge transfer kinetic with the MO molecules. The optical absorption spectroscopy analysis of the samples that is shown in Figure 7 further confirms such modification of the optical

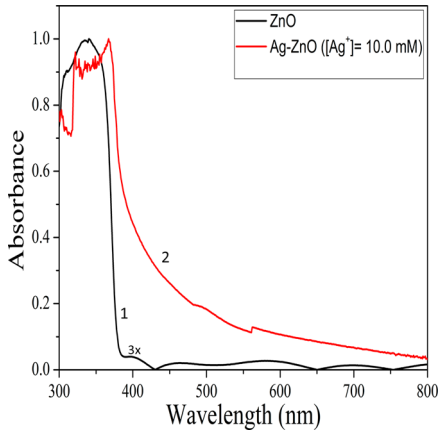

Figure 7. Normalized-optical absorption spectrum of undoped-ZnO nanorods (1) and A-ZNRs with optimum Ag+ ion doping (2), which is the the sample that was used for photocatalytic application. The undoped-ZnO nanorods were multiplied three times for a normalization process.

absorption properties of the ZnO upon the presence of Ag dopant. A significant red-shift in the band gap of the ZnO and effective improvement in the optical density of the A-ZNRs over the undoped-ZnO nanorods (see curve 2) reflects a substantial improvement of the photoactivity of the A-ZNRs. Thus, enhances the photocatalytic property of the A-ZNRs system. The possibility of Ag crystallites residing on the surface of the A-ZNRs could also play a critical role in the charge transfer kinetic between A-ZNRs and MO molecules because the Ag nanostructure itself is a highly oxidating agent. In addition, during the light absorption by the ZnO, photoexcited-electrons in the ZnO may be transferred to Ag and produce more active charge transfer kinetic between the two systems.[29] Thus, enhanced photodegradation efficiency will be obtained.

We have also evaluated the stability property of the A-ZNRs in the photocatalytic degradation of MO by examining its performance under multiple applications in the photo-degradation experiment. In typical procedure, we reused the A-ZNRs that have been applied in the degradation of MO to degrade a fresh MO solution of the same concentration. The results are shown in Figure 8. As the Figure 8 shows, the A-ZNRs exhibits excellent stability property by demonstrating insignificant change in the performance even though after being used for 5 times in the degradation of fresh solution of MO. For example, the fresh A-ZNRs sample indicates the photocatalytic degradation of up to 72.085% for a 60 min reaction time. The

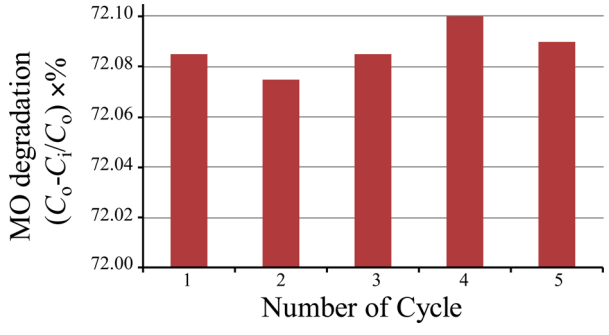

Figure 8. Stability performance of A-ZNRs in multiple used in the degradation of MO. C_o and C_i are the initial and the final concentration of MO (60 min).

dx.doi.org/10.1021/co400157m | ACS Comb. Sci. 2014, 16, 314−320

performance after being 5 times in the reaction is approximately 72.095%, confirming the excellent stability of A-ZNRs. This infers that the A-ZNRs feature large active sites on the surface facilitating a dynamic catalytic reaction. Thus, it may be unsaturated even though being used extensively. The A-ZNRs system may find a potential use for a green photocataltyic degradation of pollutant.

4. CONCLUSION

A-ZNRs have been successfully grown directly on the FTO surface via a microwave assisted hydrolysis process. In a typical procedure, high-density A-ZNRs can be realized on the FTO surface within only 30 s. A-ZNRs adopts hexagonal cross-section morphology and is characterized by a rough, rugged surface both on the inner or outer surfaces and the nanotube's edge with a visible Ag interstitial growth on the nanotube structure. Its length, shell thickness, and hexagonal edge length are 95, 15, and 40 nm, correspondingly. The A-ZNRs exhibited excellent heterogeneous photocatalytic property in the photo-degradation of MO with efficiency as high as 21.6% μg^{-1} W^{-1} within 60 min, which is 10^3 order higher than the reported results. This result is equivalent to ToF of 360 mol mol^{-1} h^{-1}. The sample also shows excellent photocataltyic stability by demonstrating a stable performance although being reused for 5 times in the degradation of a fresh MO solution. Highly defected surface structure and high surface area as well as improvement of the light absorption and the oxidation property of the A-ZNRs by the presence of Ag nanostructure could be the reason for their high-photocatalytic property. The A-ZNRs might find a potential use for a green photo catalysis and photoelectrochemical devices.

AUTHOR INFORMATION

Corresponding Author

*E-mail: akrajas@ukm.edu.my. Tel.: +603 8911 8547. Fax.: +603 8925 0439.

Notes

The authors declare no competing financial interest.

ACKNOWLEDGMENTS

The authors are grateful for the financial support received from the Ministry of Higher Education in Malaysia, under the Research Fundamental (FRGS/2/2013/SG02/UKM/02/8) and HiCOE Project and the Universiti Kebangsaan Malaysia under DIP-2012-16 and GUP-2013-030 schemes.

REFERENCES

(1) Fox, M. A.; Dulay, M. T. Heterogeneous photocatalysis. *Chem. Rev.* **1993**, *93*, 341−357.
(2) Kong, X. Y.; Ding, Y.; Wang, Z. L. Metal-semiconductor Zn−ZnO core-shell nanobelts and nanotubes. *J. Phys. Chem. B* **2004**, *108*, 570−574.
(3) Balouch, A.; Ali Umar, A.; Shah, A. A.; Mat Salleh, M.; Oyama, M. Efficient heterogeneous catalytic hydrogenation of acetone to isopropanol on semihollow and porous palladium nanocatalyst. *ACS Appl. Mater. Interfaces* **2013**, *5*, 9843−9849.
(4) Balouch, A.; Umar, A. A.; Tan, S. T.; Nafisah, S.; Md Saad, S. K.; Salleh, M. M.; Oyama, M. Fibrous, ultra-small nanorod-constructed platinum nanocubes directly grown on the ITO substrate and their heterogeneous catalysis application. *RSC Adv.* **2013**, *3*, 19789−19792.
(5) Lao, C. S.; Gao, P. M.; Sen Yang, R.; Zhang, Y.; Dai, Y.; Wang, Z. L. Formation of double-side teethed nanocombs of ZnO and self-catalysis of Zn-terminated polar surface. *Chem. Phys. Lett.* **2006**, *417*, 358−362.
(6) Umar, A. A.; Oyama, M. Synthesis of palladium nanobricks with atomic-step defects. *Cryst. Growth Des.* **2008**, *8*, 1808−1811.
(7) Yang, Y.; Yang, Y.; Wu, H.; Guo, S. Control of the formation of rod-like ZnO mesocrystals and their photocatalytic properties. *CrystEngComm* **2013**, *15*, 2608−2615.
(8) Wang, C.; Ranasingha, O.; Natesakhawat, S.; Ohodnicki, P. R.; Andio, M.; Lewis, J. P.; Matranga, C. Visible light plasmonic heating of Au−ZnO for the catalytic reduction of CO_2. *Nanoscale* **2013**, *5*, 6968−6974.
(9) Shao, M.; Ning, F.; Wei, M.; Evans, D. G.; Duan, X. Hierarchical nanowire arrays based on ZnO core−layered double hydroxide shell for largely enhanced photoelectrochemical water splitting. *Adv. Funct. Mater.* **2014**, *24*, 580−586.
(10) Fu, D.; Han, G.; Chang, Y.; Dong, J. The synthesis and properties of ZnO−graphene nano hybrid for photodegradation of organic pollutant in water. *Mater. Chem. Phys.* **2012**, *132*, 673−681.
(11) Kumar, R.; Kumar, G.; Umar, A. ZnO nano-mushrooms for photocatalytic degradation of methyl orange. *Mater. Lett.* **2013**, *97*, 100−103.
(12) Vu, T. T.; del Río, L.; Valdés-Solís, T.; Marbán, G. Stainless steel wire mesh-supported ZnO for the catalytic photodegradation of methylene blue under ultraviolet irradiation. *J. Hazard. Mater.* **2013**, *246−247*, 126−134.
(13) Lei, Y.; Zhao, G.; Liu, M.; Zhang, Z.; Tong, X.; Cao, T. Fabrication, characterization, and photoelectrocatalytic application of ZnO nanorods grafted on vertically aligned TiO_2 nanotubes. *J. Phys. Chem. C* **2009**, *113*, 19067−19076.
(14) Hung, S.-T.; Chang, C.-J.; Hsu, M.-H. Improved photocatalytic performance of ZnO nanograss decorated pore-array films by surface texture modification and silver nanoparticle deposition. *J. Hazard. Mater.* **2011**, *198*, 307−316.
(15) Tan, S. T.; Umar, A. A.; Balouch, A.; Yahaya, M.; Yap, C. C.; Salleh, M. M.; Oyama, M. ZnO nanocubes with (101) basal plane photocatalyst prepared via a low-frequency ultrasonic assisted hydrolysis process. *Ultrason. Sonochem.* **2014**, *21*, 754−760.
(16) Wang, H.; Li, G.; Jia, L.; Wang, G.; Tang, C. Controllable preferential-etching synthesis and photocatalytic activity of porous ZnO nanotubes. *J. Phys. Chem. C* **2008**, *112*, 11738−11743.
(17) Xie, W.; Li, Y.; Sun, W.; Huang, J.; Xie, H.; Zhao, X. Surface modification of ZnO with Ag improves its photocatalytic efficiency and photostability. *J. Photochem. Photobiol. A* **2010**, *216*, 149−155.
(18) Song, C.; Lin, Y.; Wang, D.; Hu, Z. Facile synthesis of Ag/ZnO microstructures with enhanced photocatalytic activity. *Mater. Lett.* **2010**, *64*, 1595−1597.
(19) Liu, H. R.; Shao, G. X.; Zhao, J. F.; Zhang, Z. X.; Zhang, Y.; Liang, J.; Liu, X. G.; Jia, H. S.; Xu, B. S. Worm-like Ag/ZnO core−shell heterostructural composites: Fabrication, characterization, and photo-catalysis. *J. Phys. Chem. C* **2012**, *116*, 16182−16190.
(20) Ridha, N. J.; Umar, A. A.; Alosfur, F.; Jumali, M. H. H.; Salleh, M. M. Microwave-assisted hydrothermal method for porous zinc oxide nanostructured-films. *J. Nanosci. Nanotechnol.* **2013**, *13*, 2667−2674.
(21) Tan, S. T.; Umar, A. A.; Yahaya, M.; Salleh, M. M.; Yap, C. C.; Nguyen, H.-Q.; Dee, C.-F.; Chang, E. Y.; Oyama, M. Formation of a multi-arm branched nanorod of ZnO on the Si surface via a nanoseed-induced polytypic crystal growth using the hydrothermal method. *Sci. Adv. Mater.* **2013**, *5*, 803−809.
(22) Umar, A. A.; Oyama, M. A seed-mediated growth method for vertical array of single-crystalline CuO nanowires on surfaces. *Cryst. Growth Des.* **2007**, *7*, 2404−2409.
(23) Umar, A. A.; Oyama, M. A cast seed-mediated growth method for preparing gold nanoparticle-attached indium tin oxide surfaces. *Appl. Surf. Sci.* **2006**, *253*, 2196−2202.
(24) Umar, A. A.; Oyama, M. Attachment of gold nanoparticles onto indium tin oxide surfaces controlled by adding citrate ions in a seed-mediated growth method. *Appl. Surf. Sci.* **2006**, *253*, 2933−2940.
(25) Cobley, C. M.; Xia, Y. Engineering the properties of metal nanostructures via galvanic replacement reactions. *Mater. Sci. Eng.,R* **2010**, *70*, 44−62.

(26) Sun, Y.; Riley, D. J.; Ashfold, M. N. Mechanism of ZnO nanotube growth by hydrothermal methods on ZnO film-coated Si substrates. *J. Phys. Chem. B* **2006**, *110*, 15186−15192.
(27) Chu, D.; Masuda, Y.; Ohji, T.; Kato, K. Formation and photocatalytic application of ZnO nanotubes using aqueous solution. *Langmuir* **2009**, *26*, 2811−2815.
(28) Arenz, M.; Mayrhofer, K. J. J.; Stamenkovic, V.; Blizanac, B. B.; Tomoyuki, T.; Ross, P. N.; Markovic, N. M. The effect of the particle size on the kinetics of CO electrooxidation on high surface area Pt catalysts. *J. Am. Chem. Soc.* **2005**, *127*, 6819−6829.
(29) Ariga, H.; Taniike, T.; Morikawa, H.; Tada, M.; Min, B. K.; Watanabe, K.; Matsumoto, Y.; Ikeda, S.; Saiki, K.; Iwasawa, Y. Surface-mediated visible-light photo-oxidation on pure TiO_2(001). *J. Am. Chem. Soc.* **2009**, *131*, 14670−14672.